

*Full Length Research Paper*

# Modeling of glow discharge controlled by a dielectric barrier

Mankour Mohamed\* and Belarbi Ahmed Wahid

Department of Electrotechnical, Faculty of Electrical Engineering, University of Sciences and Technology of Oran, Algeria.

Accepted 18 August, 2011

**Numerical calculations of spatio-temporal characteristics of the homogeneous barrier discharge in helium are performed by means of a one-dimensional fluid model. This model consists of the continuity equations for electrons, ions and excited atoms, with the current conservation equation and the electric field profile; the time evolution of the discharge current, gas voltage and the surface density of charged particles on the dielectric barrier were calculated. The simulation results showed that the peak values of the discharge current, gas voltage and electric field in the first half period are asymmetric to the second half. When the current reaches its positive or negative maximum, the electric field profile and the electron and ion densities represent similar properties to the typical glow discharge at low pressures.**

**Key words:** Atmospheric pressure glow discharge, numerical simulation, helium gas.

## INTRODUCTION

This work deals with a numerical study of glow discharge set up in the helium atmospheric pressure. This study consists of developing a monodimensional numerical model with the aim to examine the properties of this discharge.

The applicant's field of this process is a very wide (Kogelshtz, 2003) ozone generation processing of gaseous effluents, activation and processing of surface CO<sub>2</sub> laser, lamp excimer, plasma screens, etc., and they deal with numerous industrial domains, such as: electronics, textile, packaging car and manufacturing.

In recent years, many studies have been concerned with the effects of gas flow and electrode geometry on the discharge mode and characteristics. Several authors have published experimental and modeling studies of plane-parallel dielectric barrier discharge (DBD) at atmospheric pressure under specific conditions; for instance, at least one of the electrodes covered with a dielectric layer, an ac power with an appropriate frequency, atmospheric pressure glow discharges (APGDs), etc., was obtained relatively readily in helium. Helium APGDs have been studied extensively. For simplicity, many theoretical studies made an approximation that the average electron energy is constant throughout the discharge

space at any time; the value of electron energy is chosen empirically.

The line of works in the glow discharge with dielectric barrier is to turn towards a very detailed modeling of the discharge, a good modeling makes it possible to understand and predict their behavior (Roth et al., 1998, 2005; Corke et al., 2003; Kim et al., 2004; Shenton and Stevens, 2001; Golubovskii, 2003; Tendero et al., 2006; Massines et al., 2003), then the control and use of this technology in industrial needs such as: semi-conductors, panels of plasma visualization, the deposit of the thin layers, the die-sinking in micro-electronics and the treatment of surfaces (Webb et al., 2007; Montie et al., 2000; Yang, 2005; Massines et al., 1998; Singh et al., 2006).

## PHYSICAL MODEL

The functioning of this discharge which is similar to all the discharges in gas is governed and directed by a multitude of different physical phenomena from one to another but is strongly coupled. Thus, It is necessary to consider the system on the whole, and then to work out (carry out) a self-coherent modeling that will be able to take into account the coupling between the conveyance of charged particles and the kinetics of the existing states on the one hand and the electrical field on the other hand.

Thus, the model being developed allows proper

\*Corresponding author. E-mail : [mohamed\\_mdz2000@yahoo.fr](mailto:mohamed_mdz2000@yahoo.fr).

understanding of the functioning of the discharge. In this study, an attempt was made to reproduce an electrical characteristics of the discharge from the description of the involved basic physical phenomena (phenomena of electronic and ionic conveyance in gas, electrical field). These characteristics do not inform us about the intervention of the whole phenomena during the discharge.

The use of helium within the framework of this study is one of the conditions of obtaining a glow rate of charge atmospheric pressure of gas, mainly characterized by its metastable levels of potential high-energy and by its weak potential of rupture.

The reaction was taken into account in the numerical modeling and putting in plays the electrons, the ions and the natural excited particles are represented as shown in Figure 1 (Gadri, 1999).

The reaction rates of which some are presented in Figure 1, are constant depending on the electric field. The knowledge of these factors which control the density of different particles is necessary to understand and to describe the discharge.

**MATHEMATICAL MODEL**

The finest theoretical description of the particles behavior which characterized the functioning of an electrical discharge requires the resolution of the kinetics equations in entirety (frequency called equation of discharge particle conveyance) associated with each one of these particles.

Fundamental equation rendering account of the space and temporal evolution of particles density is the equation of continuity that globally takes the same form for electrons and ions. The following equations were derived:

For the electrons;

$$\frac{\partial ne(\vec{r},t)}{\partial t} + \frac{\partial(\vec{w}_e(\vec{r},t)n_e(\vec{r},t))}{\partial \vec{r}} - \frac{\partial}{\partial \vec{r}} \left[ \vec{D}_e(\vec{r},t) \frac{\partial n_e(\vec{r},t)}{\partial \vec{r}} \right] = s_e(\vec{r},t) \tag{1}$$

For the ions;

$$\frac{\partial ni(\vec{r},t)}{\partial t} + \frac{\partial(\vec{w}_i(\vec{r},t)n_i(\vec{r},t))}{\partial \vec{r}} - \frac{\partial}{\partial \vec{r}} \left[ \vec{D}_i(\vec{r},t) \frac{\partial n_i(\vec{r},t)}{\partial \vec{r}} \right] = s_i(\vec{r},t) \tag{2}$$

For the excited particles;

$$\frac{\partial n_m(\vec{r},t)}{\partial t} - \frac{\partial}{\partial \vec{r}} \left[ \vec{D}_m(\vec{r},t) \frac{\partial n_m(\vec{r},t)}{\partial \vec{r}} \right] = S_m(\vec{r},t) \tag{3}$$

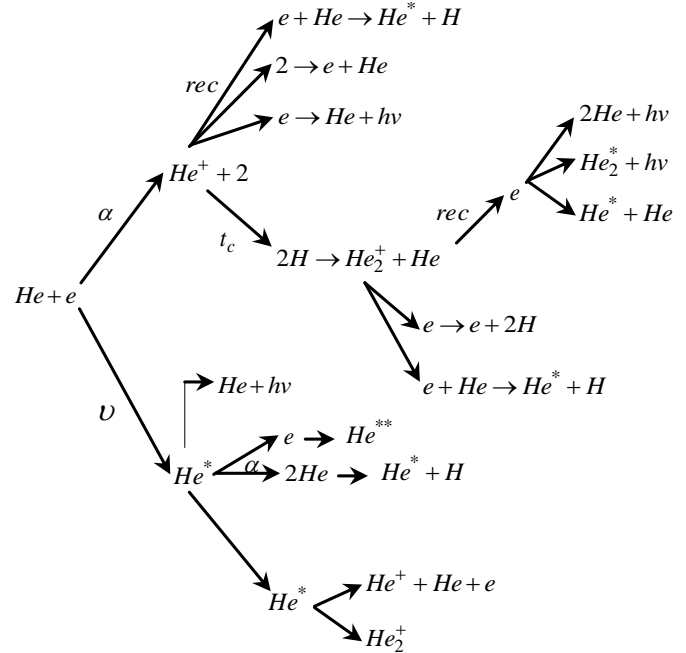


**Figure 1.** The process of reaction and the disappearance of different particles.

which permit us to determine the space temporal evolution of the electronic and ionic densities subject to the knowledge of the running back speed, diffusion coefficient and frequencies of ionization of each charged particle.

The three aforementioned equations are named convection-diffusion equation, because they are composed of the terms convective (of the 1st rank with regard to the space shunted) and diffusion (of the 2nd rank with regard to the space shunted).

In glow discharge, the space charged due to the ions and electrons presence is sufficient to distort the geometrical electric field. This phenomenon should be described by coupling the equations of electric and ionic conveyance with the equation of Poisson for the electric field, and the equation of Poisson is written as:

$$\vec{\nabla} \cdot \epsilon_r E = \frac{e}{\epsilon_0} (n_i - n_e - n_n) \tag{4}$$

The equation of Boltzmann is coupled with the one of Poisson from an auto coherent electrical model of the discharge.

**Macroscopic approach (Fluid models)**

The conveyance of the charge particles in this approach is characterized by average size, then the density, the average speed and average energy of the particles. The equation of Boltzmann is then substituted by three

equations which described the space-temporal evolution of three average values.

### Fluid model with the two moments

The developed model in this research was based on the resolution of the first two moments of Boltzmann's equation. In this model, the first 2 conveyance equations are:

1. Continuity equation
2. Conveyance equation of the quantity of movement coupled with the Poisson equation.

To be able to suppress the equation of energy, it is necessary to use the local field approximation.

The numerical model developed in this research is fluid and mono-dimensional. The aim of a fluid model is to give the appropriate qualitative tendencies which enable us to know the preponderant physical phenomena that affect the discharge at the level of the actuator DBD.

### Source terms of conveyance equations

The expressions of the source terms of electrons, ions and of the metastable contain the reactions rates (noted  $k_i$ ) and the ionization frequencies and excitation besides the different particle density (Massines et al., 1998; Andrade et al., 2008).

#### Electron

$$S_e = \nu n_e + n_{x1}(k_{11}n_{x1}) - n_{p1}n_e(k_4 + k_5n_e + k_6n_{He}) - N_{p2}n_e(k_7 + k_8 + k_2n_{He} + k_9n_e) - n_{p3}n_e(k_{10} + k_{11}n_e) \quad (5)$$

#### Atomic ions $He^+$

$$S_{p1} = \nu n_e + k_{11}(n_{x1})^2 - n_{p1}n_e((k_4 + k_5n_e + k_6n_{He}) - n_{p1}k_1(n_{He})^2) \quad (6)$$

#### Molecular ions $He_2^+$

$$S_{p2} = n_{p1}k_1(n_{He})^2 - n_{p2}n_e(k_2n_{He} + k_7 + k_8 + k_9n_e) \quad (7)$$

### Source term of the excited species $He(2^3S)$

$$S_{x1} = \nu_1n_e + n_{p2}n_e k_8 - n_{x1}(k_3(n_{He})^2 + k_{10}n_e + k_{11}n_{x1}) \quad (8)$$

where  $n_e$ ,  $n_{p1}$ ,  $n_{p2}$ ,  $n_{He}$  designate, respectively the density of the electrons atomic and molecular ions of helium, where  $n_{x1}$  designates (indicates) the helium density.  $He(2^3S)$  is the charged particles and the rates  $k_i$  are defined in Table 1 (Golubovskii, 2003; Hill and Herman, 1993; Quinteros et al., 1995; Yuan and Raja, 2003).

### NUMERICAL MODEL

The continuity equation from the method of the finished differences was solved based on the discretization diagram of Sharfetter and Gummel (1969). Its main advantage was related to its stability and to the fact that it can be delivered in a continuous manner or situation in which either the term "Shunt", or the term diffusion of the current of the charged particle is dominant. This diagram enables us to discredit implicitly the equation of continuity and to break loose from constraints of pace in time imposed in the case of explicit discretization.

The discretization of density of the charged particles and the flux as well as that of Poisson equation is as follows:

### Discretization of the convergence equations

Generally, we can not solve the heavily coupled systems, constituted of the first two instances of Boltzmann's equation and one of Poisson's in a simple and direct manner. The problem is to draw as near as possible the exact values to the solution. The chosen method is the method of the finished differences according to the diagram of Sharfetter and Gummel (1969) for the developed conveyance at the lead for semi-conductors modeling.

### Discretization of density of the charged particles and of the flux

The densities of the charged particles are defined at the  $(i, j)$  cell core (Figure 2). In the equation of continuity and in the transfer of the movement quantity, the flux of the charged particles following the "x" axe and the one of the "Y" axe are defined between the  $(i, j)$  and  $(i+1, j)$  and  $(i, j)$  and  $(i, j+1)$  points, respectively.

In this method of Sharfetter and Gummel, we supposed

**Table 1.** Assessment of the reactions in helium.

Reaction	Symbol	Rate of reaction (cm <sup>6</sup> s <sup>-1</sup> )
<b>Reaction to three bodies</b>		
$He^+ + 2He \rightarrow He_2^+ + He$	$k_1$	$6.3 \times 10^{-32}$
$He_2^+ + e + He \rightarrow He_2^* + He$	$k_2$	$5 \times 10^{-27}$
$He(2^3S) + He \rightarrow He_2^* + He$	$k_3$	$2.5 \times 10^{-34}$
<b>Recombination</b>		
$He^+ + e \rightarrow He + hv$	$k_4$	$2 \times 10^{-12}$
$He^+ + 2e \rightarrow He + e$	$k_5$	$7.1 \times 10^{-20}$
$He^+ + e + He \rightarrow He^* + He$	$k_6$	$1 \times 10^{-27}$
$He_2^+ + e \rightarrow He_2^* + hv$	$k_7$	$5 \times 10^{-10}$
$He_2^+ + e \rightarrow He(2^3S) + He$	$k_8$	$5 \times 10^{-9}$
$He_2^+ + e \rightarrow 2He + e$	$k_9$	$2 \times 10^{-20}$
<b>Reaction to two bodies</b>		
$He(2^3S) + e \rightarrow He + e$	$k_{10}$	$2.9 \times 10^{-9}$
$He(2^3S) + He(2^3S) \rightarrow e + He^+$	$k_{11}$	$2.9 \times 10^{-9}$

that the particle flux is constant between two successive nodes of the maillage. Figure 2 shows the integration of the conveyance equation (that is, analytic) which confers or bestows a very good stability on the model. For instance, we start by following the conveyance equation X:

$$\Gamma = s \cdot \frac{\mu \cdot E}{D} (n \cdot D) - \frac{\partial(nD)}{\partial x} \quad (9)$$

where  $\mu$  and  $D$  are the mobility and diffusion coefficient, and  $S$  is equal to -1 and 1 for the electrons and ions, respectively.

This study takes as a solution the following equation:

$$nD = s \cdot \frac{D}{\mu \cdot E} \Gamma + C \exp\left(s \frac{\mu \cdot E}{D} x\right) \quad (10)$$

The densities of the charged particles are defined at the center of  $(i, j)$  cells. We will have for example, the same value  $\Gamma_{x,i+1/2,j}$  of the flux between  $(i, j)$  and  $(i+1, j)$  nodes, as soon as the discretization following the finished difference gives off:

$$n_{i,j} D_{i,j} = s \cdot \frac{D_{i+1/2,j}}{\mu_{i+1/2,j} \cdot E} \Gamma_{i+1/2,j} + C \exp\left(s \frac{\mu_{i+1/2,j} \cdot E_{i+1/2,j}}{D_{i+1/2,j}} x_{i,j}\right) \quad (11)$$

$$n_{i+1,j} D_{i+1,j} = s \cdot \frac{D_{i+1/2,j}}{\mu_{i+1/2,j} \cdot E} \Gamma_{i+1/2,j} + C \exp\left(s \frac{\mu_{i+1/2,j} \cdot E_{i+1/2,j}}{D_{i+1/2,j}} x_{i,j}\right) \quad (12)$$

If equations 11 and 12 are subtracted,  $C$  will be obtained:

$$C \exp\left(s \frac{\mu_{i+1/2,j} \cdot E_{i+1/2,j}}{D_{i+1/2,j}} x_{i,j}\right) = \frac{n_{i+1,j} D_{i+1,j} - n_{i,j} D_{i,j}}{\exp\left(s \frac{\mu_{i+1/2,j} \cdot E_{i+1/2,j}}{D_{i+1/2,j}} x_{i,j}\right) - 1} \quad (13)$$

Paying

$$Z_{i+1/2,j} = s \frac{\mu_{i+1/2,j} \cdot E_{i+1/2,j}}{D_{i+1/2,j}} \Delta x_{i,j} \quad (14)$$

The expression of the following flux  $X$  was written in the discretization of the finished differences, according to the exponential diagram of Sharfetter and Gummel is as follows:

$$\Gamma_{x,i+1/2,j} = -\frac{1}{x} D_{i+1/2} (f_1(z_{x,i+1/2,j}) n_{i+1,j} - f_2(z_{x,i+1/2,j}) n_{i,j}) \quad (15)$$

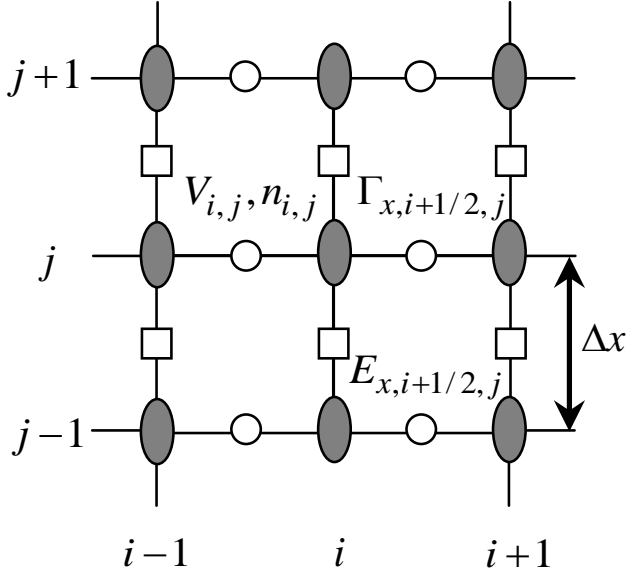


Figure 2. Used maillage in the model.

After  $F_1(2)$  and  $F_2(2)$  have been defined by:

$$f_1(z) = \frac{z}{\exp(z) - 1} \quad (16)$$

$$f_2(z) = \frac{z \exp(z)}{\exp(z) - 1} = f_1(z) + z \quad (17)$$

For  $z \neq 0$  and  $F_1(0) = F_2(0) = 1$ , the expression of flux (the flux expression) in the Y direction has the same form.

We replace in the equation of continuity the flux by their expression which is a linear combination of densities and the following equation was obtained which is a linear combination between the five neighbors' points.

$$a_{i,j}^E n_{i+1,j} + a_{i,j}^w n_{i-1,j} + a_{i,j}^N n_{i,j+1} + a_{i,j}^S n_{i,j-1} + a_{i,j}^c n_{i,j} = A_{i,j} \quad (18)$$

The coefficients inside the simulation field are defined by:

$$a_{i,j}^E = -\frac{2\Delta t \cdot D_{i+1/2,j}}{\Delta x_i (\Delta x_i + \Delta x_{i-1})} f_1(z_{x,i+1/2,j}) \quad (19)$$

$$a_{i,j}^w = -\frac{2\Delta t \cdot D_{i-1/2,j}}{\Delta x_{i-1} (\Delta x_i + \Delta x_{i-1})} f_2(z_{x,i-1/2,j}) \quad (20)$$

$$a_{i,j}^N = -\frac{2\Delta t \cdot D_{i,j+1/2}}{\Delta y_{j+1} (\Delta y_j + \Delta y_{j-1})} f_1(z_{y,i,j+1/2}) \quad (21)$$

$$a_{i,j}^S = -\frac{2\Delta t \cdot D_{i,j-1/2}}{\Delta y_{j-1} (\Delta y_i + \Delta y_{i-1})} f_1(z_{y,i,j-1/2}) \quad (22)$$

$$a_{i,j}^c = 1 - a_{i-1,j}^E - a_{i+1,j}^w - a_{i,j-1}^N - a_{i,j+1}^S \quad (23)$$

$$A_{i,j} = n_{i,j}^k + \Delta t S_{i,j} \quad (24)$$

For the surface (space) between dielectric and gas, the expression of the electronic flux was defined by:

$$(\Gamma_e \cdot n)_{i,j} = a_{i,j} \cdot \mu_{i,j} \cdot E_{i,j} \cdot n_{i,j} + \frac{v_{th,i,j} \cdot n_{i,j}}{4} - \gamma \cdot (\Gamma_p \cdot n)_{i,j} \quad (25)$$

And the coefficient expressions are:

$$a_{i,nd}^E = a_{i,nd}^w = a_{i,nd}^S = 0 \quad (26)$$

$$a_{i,nd}^n = -\frac{2\Delta t \cdot D_{i,j+1/2}}{\Delta y_{nd}} f_1(z_{y,i,j+1/2}) \quad (27)$$

$$a_{i,j}^c = 1 - a_{i,j-1}^N + \frac{2\Delta t}{\Delta y_{nd}} a_{i,nd} \cdot \mu_{i,j} \cdot E_{y,i,nd} + \frac{2\Delta t}{\Delta y_{nd}} v_{th} \quad (28)$$

$$a_{i,j}^c = 1 - a_{i-1,j}^E - a_{i+1,j}^w - a_{i,j-1}^N - a_{i,j+1}^S \quad (29)$$

Discretization of the Poisson's equation was given as :

$$\bar{\nabla} \cdot \epsilon_r E = \frac{e}{\epsilon_0} (n_i - n_e) \quad (30)$$

In the discretization of the finished differences, the "Laplacian" of the potential was written as follows:

$$\frac{\partial^2 V}{\partial x^2} \Big|_{i,j} = \frac{V_{i+1,j} + V_{i-1,j} - 2V_{i,j}}{\Delta x^2} \quad (31)$$

$$\frac{\partial^2 V}{\partial y^2} \Big|_{i,j} = \frac{V_{i,j+1} + V_{i,j-1} - 2V_{i,j}}{\Delta y^2} \quad (32)$$

### Conditions to the limits

We assumed that the flux of the charged particles towards the sides of the field of simulation is worthless (nul), thus, we translated it by the conditions to the symmetric limits  $\Gamma_e \vec{n} = 0$ . But the flux of the charged particles towards the dielectric was written under the form:

$$\varphi_{e,i} = A n_{e,i} w_{e,i} + \frac{n_{e,i} v_{th,e,i}}{4} \quad (33)$$

**Table 2.** Transport parameters used in helium.

Transport parameter	Values
Ions mobility $\mu_i$	$(8 \times 10^3/p)1.8 \times 10^{-3} E/p \text{ cm}^2\text{V}^{-1}\text{s}^{-1}$ , for $E/p \leq 25 \text{ cm}^{-1}\text{torr}^{-1}$ $(4.1 \times 10^4/p\sqrt{E/p} [1-27.44/E/p^{1.5}]) \text{ cm}^2\text{V}^{-1}\text{s}^{-1}$ , For $E/p > 25 \text{ cm}^{-1}\text{torr}^{-1}$
Electrons mobility $\mu_{ie}$	$(e/m_e u_{en}) \text{ cm}^2\text{V}^{-1}\text{s}^{-1}$ and $u_{en} = 10^2 \text{ /s}$
Ions diffusion $D_i$	$500 \text{ cm}^2/\text{s}$
Electrons diffusion $D_e$	$(KT_e/e) \mu_e \text{ cm}^2/\text{s}$

With  $w_{e,i} = \pm \mu_{e,i} E$ .  $n_{e,i}$  is the electrons or ions (i) density at the surface of the side,  $w_{e,i}$  is the derive speed, which is a parameter that is equal to 1 if  $w_{e,i}$  is directed towards the side if not equal to zero.

## RESULTS AND DISCUSSION

In our model, the series of equations mentioned earlier are solved numerically, and by discretization. Equations 1 to 4 were performed in accordance with semi-implicit Scharfetter-Gummel scheme (Scharfetter and Gummel, 1969). The mobility and diffusion coefficient used were the same as those in these studies (Roy and Gaitonde, 2005; Shi, 2003). The photoionization contribution was not taken into account in this model. As the initial condition, we assumed that the electron density and the atomic ion density are equal to each other and uniformly distributed in the discharge region  $n_e(r,0) = n_i(r,0) = 10^7 \text{ cm}^{-3}$ , while the molecular ion density and the excited atom density are both  $10^2 \text{ cm}^{-3}$ . The spacing between the two coaxial electrodes is 6 mm; a sinusoidal voltage was externally applied to the inner electrode, its amplitude and frequency were 2 kV and 50 kHz, respectively (Table 2).

Figures 3 and 4 showed the temporal evolution of the total discharge current and the gas voltage during a typical cycle. It can be seen that there is one current peak in each half cycle of the applied voltage. Different from the parallel-plate configuration, the current peak in various half periods loses its original shape. The current maximum of 0.0022 A in the first half is different from the second, which is only 0.0014 A. In addition, the pulse width of the discharge current in the latter half period was wider than that in the former. It is due to the fact that in the first half, the discharge cathode is the outer electrode with a big radius so that the volume of ionization region in the cathode sheath is also very large, leading to a strong current gathering; while in the latter half period, the discharge cathode is the inner wire electrode with a very much smaller radius. Although in the latter case the sheath electric field is much stronger than that in the former, the volume of the ionization region is however, so

small that it leads to a smaller current peak. The blue line in Figure 3 represented the time evolution of the gas voltage with the applied voltage during a typical cycle. At the initial moment, the applied voltage was zero, and the gas voltage was not zero but equal to the memory voltage produced by the charged particles accumulated on the dielectric. As the applied voltage increases, the gas voltage also increases until it reaches the breakdown voltage, then, the gas is punctured and starts to discharge. Meanwhile, the charges accumulated on the dielectric produce a reverse electric field, making the gas voltage drop and leading to a termination of the gas discharge. In the latter half period, due to the reversal of the applied voltage, the electric field produced by the accumulated charges has the same direction as the applied field, so it reduces the threshold applied voltage for starting the next discharge. Furthermore, since the breakdown during the latter half period happened in the cathode sheath near the inner wire electrode, where the electric field is strong correspondingly, it is easier to puncture, and therefore the breakdown voltage in the latter half period is lower than that in the former half period. As a result of the higher discharge current during the former half period, the accumulation seed of charged particles on the dielectric barrier is fast. Then, the gas voltage drops rapidly and the discharge was suppressed quickly and consequently, the discharge current pulse is narrow. However, during the latter half period, since the discharge current was low, the accumulation speed of charged particles on the dielectric was also low. Thus, the gas voltage changes slowly and its suppressing effect on discharge is small, so the current pulse is wide.

Figures 5 to 10 illustrated the spatial distributions of the electric field, the electron and the ion as well as the excited atom densities when the discharge current reaches its positive or negative maximum during the cycle. When the discharge happens in the former half period, the cathode sheath was formed near the dielectric barrier covering the outer electrode. There obviously existed a cathode fall, a negative glow region, a Faraday dark region and a plasma positive column. This showed a similar feature to the typical glow discharge at low pressures. In the cathode fall, the electric field can be up to 260 V/cm and then decreases linearly from the cathode. The maximal ion density in this region is  $4.5 \times 10^8 \text{ cm}^{-3}$

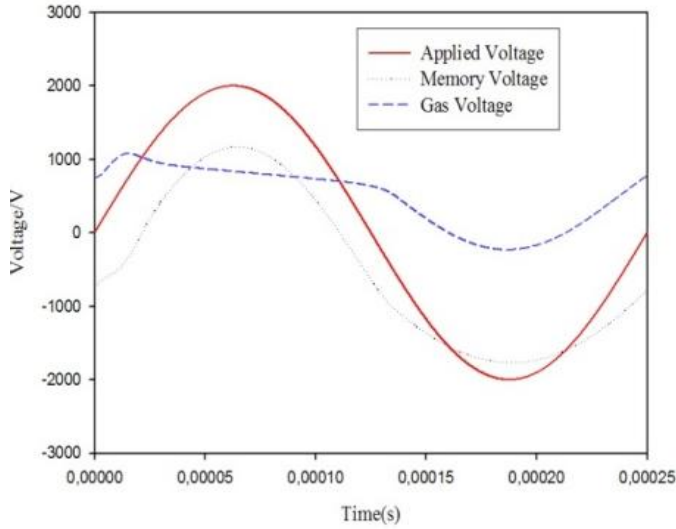


Figure 3. Evolution of the gas voltage in a typical cycle.

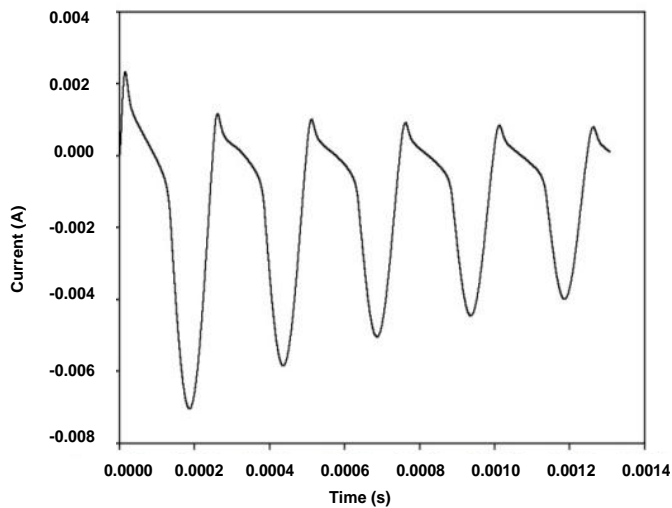


Figure 4. Evolution of the total discharge current in a typical cycle.

and the width of the cathode fall is about 0.05 cm. The width of the negative glow region and the faraday dark region is about 0.15 cm. The electron density showed a negative glow region with a peak value of  $4.1 \times 10^8 \text{ cm}^{-3}$ . In other words, when the current reaches a peak during the former half period, the maximal electron density does not occur near the sheath but near the inner electrode. Due to the axial symmetry, the current density near the inner wire electrode was the highest. In the plasma positive column, the electric field is quite low, about 30 V/cm. The electron and ion densities are nearly equal to each other. Due to the asymmetry of discharges, the densities are not uniform in the plasma region but increases gradually from the outer to the inner electrode.

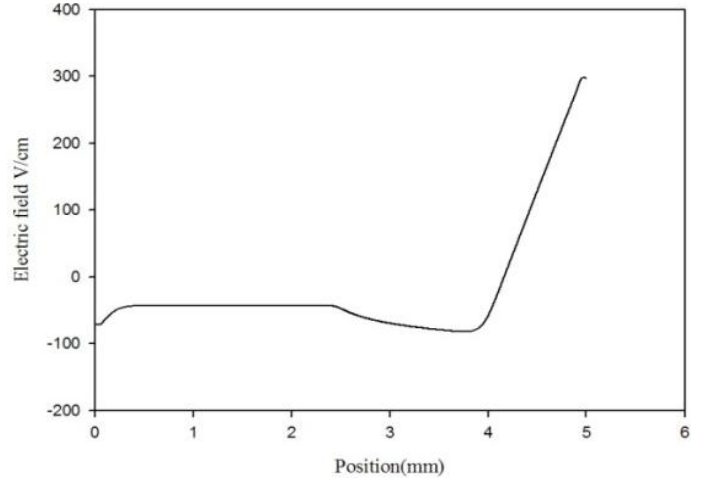


Figure 5. The spatial distribution of the electric field.

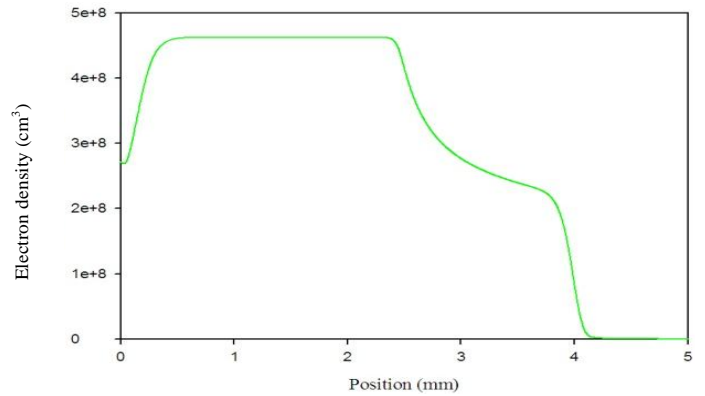


Figure 6. The spatial distribution of electron density.

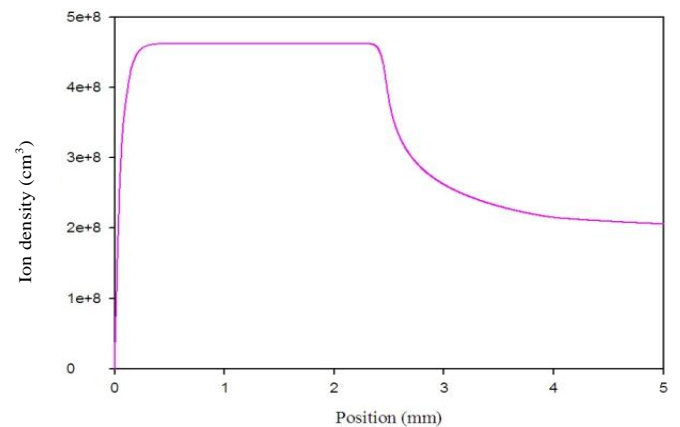
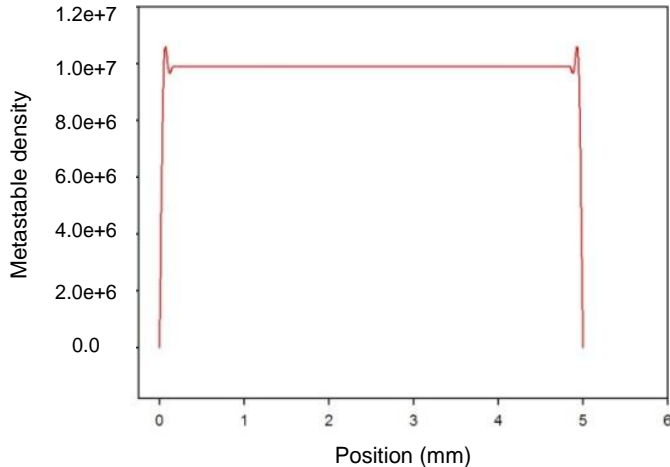
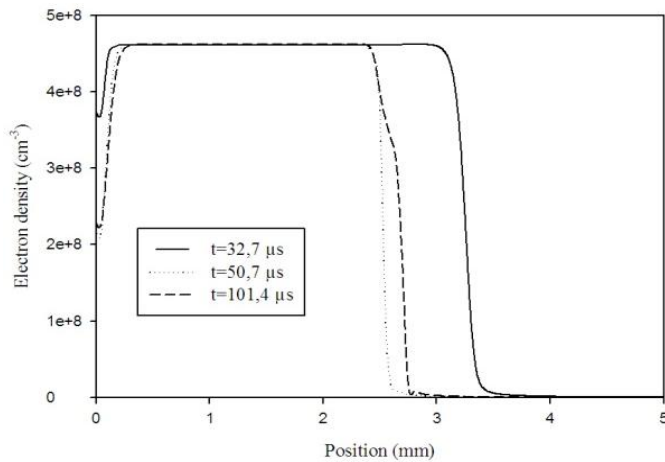


Figure 7. The spatial distribution of ion density.

The latter half period when the current reaches the maximum, the cathode sheath is formed near the inner electrode. Obviously there exist the cathode fall, the



**Figure 8.** The spatial distribution of metastable density.



**Figure 9.** The spatial distribution of electron density for  $t$  equal 32.7, 50.7 and 101.4  $\mu\text{s}$ .

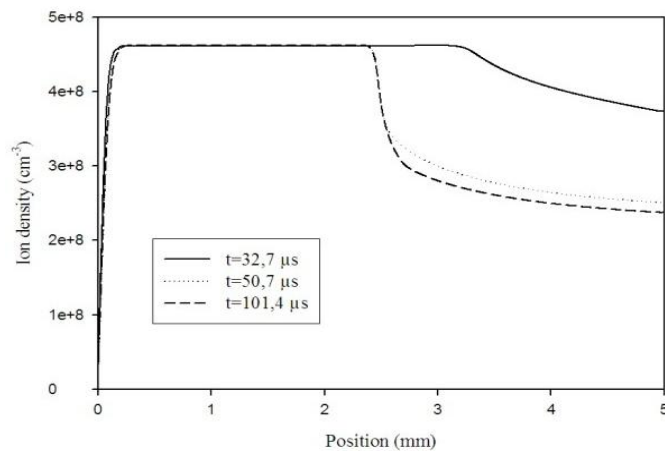


**Figure 10.** The spatial distribution of ion density for  $t$  equal 32.7, 50.7 and 101.4  $\mu\text{s}$ .

negative glow region and the positive column. In the cathode sheath, the electric field intensity is 285 V/cm in maximum and showed a tendency to reduce linearly. The thickness of the sheath is about 0.03 cm and the ion density can be up to  $4.7 \times 10^8 \text{ cm}^{-3}$ . The maximal electron density of  $4.9 \times 10^8 \text{ cm}^{-3}$  appears at the boundary near the sheath. In the plasma positive column, the electric field intensity is small and keeps almost steady; while the electron and ion density are equal to each other,  $4 \times 10^8 \text{ cm}^{-3}$ . The distribution of the excited atom density did not change much during the former and the latter half-period. The maximal densities (about  $1 \times 10^7 \text{ cm}^{-3}$ ) both appeared in the region near the inner wire electrode. The excited atom density decreased in the direction from the inner to the outer electrode.

## Conclusion

Based on the one-dimensional and self-consistent fluid model, the characteristics of the dielectric barrier glow discharge in pure helium at atmospheric pressure generated between two coaxial electrodes was numerically investigated. In calculation, we considered the elementary ionization and excitation processes in pure helium. Under the drift-diffusion approximation, by solving the one-dimensional continuity equations for electrons, ions and excited atoms, together with the current conservation equation, the simulation results showed the spatial-temporal distributions of the electric field and the electron, ion and excited atom densities, as well as the time evolutions of the discharge current and gas voltage. At maximal discharge current, there obviously existed a cathode fall, the negative glow region and the positive column, similar to the APGD with the dielectric barrier between parallel-plate electrodes. The simulation results revealed that the peak discharge current, gas voltage and the electric field are asymmetric by comparing the first half cycle with the second. However, the manner in which the dielectric covered the electrodes on discharge current characteristics is very significant.

## REFERENCES

- Andrade FJ, Shelley JT, Wetzel WC, Webb MR, Gamez, G Hieftje SJ (2008). Atmospheric pressure chemical ionization source. *Anal. Chem.*, 80(8): 2646-2653.
- Corke TC, Jumper EJ, Post ML, Orlov D, Mclaughlin TE (2003). Application of weakly-ionized plasmas as wing flow-control devices. *AIAA Paper 2002-0350*, 41<sup>st</sup> Aerospace Sciences Meeting and Exhibit, Reno, NV, Jan. 6-9.
- Gadri RB (1999). One atmospheric glow discharge structure revealed by computer modeling. *IEEE Trans. Plasma Sci.*, 27(1): 36-37.
- Golubovskii YB, Maiorov VA, Behnke J, Behnke JF (2003). Modeling of the homogeneous barrier discharge in helium at atmospheric pressure. *J. Phys. D, App. Phys.*, 36: 39-49.
- Hill PC, Heman PR (1993). Reaction processes in  $\text{He}^+$  flash lamp. *Phys. Rev.*, 47(6): 4837-4844.
- Kim Y, Kang WS, Park JM, Hong SH, Song YH, Kim SJ (2004). Experimental and numerical analysis of streamers in pulsed corona

- and dielectric barrier discharges. *IEEE Trans. Plasma Sci.*, 32(1): 18-24.
- Kogelshtz U (2003). Dielectric-barrier discharges their history discharge physics and industrial applications. *Plasma chem. Plasma Process.*, 33(1): 1-46.
- Massines F, Messaoudi R, Mayoux C (1998). Comparison between air filamentary and helium glow dielectric barrier discharges for the polypropylene surface treatment. *Plasmas Polym.*, 3(1): 43-59.
- Massines F, Rebehi A, Decomps P, Gadri RB, Ségur P, Mayoux C (1998). Experimental and theoretical study of a glow discharge at atmospheric pressure controlled by dielectric barrier. *J. App. Phys.*, 83(6): 2950-2957.
- Massines F, Ségur P, Gherardi N, Khamphan C, Ricard A (2003). Physics and chemistry in a glow dielectric barrier discharge at atmospheric pressure: Diagnostics and modeling. *Surf. Coatings Technol.*, 8(14):174-175.
- Montie TC, Kelly-Wintenberg K, Roth JR (2000). An overview of research using the one atmosphere uniform glow discharge plasma (OAUGDP) for sterilization of surfaces and materials. *IEEE Trans. Plasma Sci.*, 28(1): 41-50.
- Quinteros T, Dewitt DR, Schuch R, Belkic D (1995). Recombination of  $D^+$  and  $He^+$  ions with low-energy free electrons. *Phys. Rev.*, 51: 1340-1349.
- Roth JR, Rahel J, Dai X, Sherman DM (2005). The physics and phenomenology of one atmosphere uniform glow discharge plasma (OAUGDP) reactors for surface treatment applications. *J. Phys. D, Appl. Phys.*, 38(4): 555-567.
- Roth JR, Sherman DM, Wilkinson SP (1998). Boundary layer flow control with a one atmosphere uniform glow discharge. *AIAA paper 98-0328*, 36<sup>th</sup> AIAA Aerospace Sciences Meeting and Exhibit, Reno, NV, Jan.12-15.
- Roy S, Gaitonde DV (2005). Modeling surface discharge effects of atmospheric RF on gas flow control. *Proceedings 43<sup>rd</sup> AIAA Aerospace Sciences Meeting*, 160: 10-13.
- Scharfetter DL, Gummel HK (1969). Large signal analysis of silicon read diode oscillator. *IEEE Trans. Electron devices ED-16*, Vol. 64.
- Shenton MJ, Stevens GC (2001). Surface modification of polymer surfaces: Atmospheric plasma versus vacuum plasma treatments. *J. Phys. D, App. Phys.*, 34(18): 2761-2768.
- Shi JJ, Kong MG (2003). Cathode fall characteristics in a dc atmospheric pressure glow discharge. *J. App. Phys.*, 94(9): 5504-5513.
- Singh KP, Roy S, Gaitond DV (2006). Modeling of dielectric barrier discharge plasma actuator with atmospheric air chemistry. *AIAA Paper 2006-3381*, 37<sup>th</sup> AIAA Plasma dynamics and lasers Conference, San Francisco, CA, June. pp. 5-8.
- Tendero C, Tixier C, Tristant P, Desmaison J, Leprince P (2006). Atmospheric pressure plasmas. *Spectrochim. Acta, Part B*, 61(7): 2-30.
- Webb MR, Andrade FJ, Hieftje GM (2007). The annular glow discharges- A small-scale plasma for solution analysis. *Anal. At. Spectrum*, 22(7): 775-782.
- Yang X (2005). Comparison of an atmospheric pressure, radio-frequency discharge operating in the  $\alpha$  and  $\gamma$  modes, *Plasma Sources Sci.*, 19(2): 314-320.
- Yuan X, Raja LL (2003). Computational study of capacitively coupled high-pressure glow discharges in helium. *IEEE Trans. Plasma Sci.*, 31(4): 495-503.